New Hypotheses for Mercury Porosimetry with Percolation Approach

New hypotheses of no coalescence and no entrapment are proposed for mercury intrusion and extrusion. Pore structures are represented by a two-dimensional lattice for bond percolation and the Rayleigh distribution function taken for the pore size distribution. Different modes of hysteresis are found with the new hypotheses and the effect of accessible probability on the hysteresis loop is analyzed. A bimodal size distribution with micropores and macropores is analyzed by considering the extent of overlapping and the sequence of connection between both distributions. Mercury entrapment is also predicted by considering the pressure difference between the applied and assigned pressures, as determined by the Washburn equation, as a parameter for mercury breakage. The applicability of the proposed hypotheses is demonstrated by showing that experimental data on an α-alumina sample could be well correlated.

Churl-Young Park
Son-Ki Ihm
Department of Chemical Engineering
Korea Advanced Institute of Science
and Technology
Seoul, Korea

Introduction

In mercury porosimetry, the intruded mercury volume is measured as a function of the applied pressure, which for a cylindrical pore is related to the pore radius by the Washburn equation:

$$P = \frac{-2\delta \cos\theta}{r}$$

where P is the applied pressure, δ the surface tension, θ the contact angle, and r the pore radius. The data obtained by this method can in practice be analyzed when the pore structure is assumed. The capillary tube model (CTM) is widely used, in which the bundles of capillary tubes are individually connected to the external surface of material without being intersected (Dullien, 1979). With the CTM, however, hysteresis and mercury entrapment cannot be expected.

A paper by Broadbent and Hammersley opened the gate of percolation theory in 1957. The key concept and its application appeared in review papers (Shante and Kirkpatrick, 1971; Essam, 1980). Porous material may be defined as a regular lattice, such as a simple network (Androutsopoulos and Mann, 1979; Mason, 1982), a cubic lattice (Wall and Brown, 1981; Yanuka et al., 1986; Zhdanov et al., 1987), or a Bethe lattice (Reyes, 1985; Mishra and Sharma, 1988; Rafi and Tirrell, 1988). The lattice is composed of a set of sites interconnected by bonds, and the bonds (or sites) are occupied with a fixed probability for percolation. As a result, percolation theory deals with the clusters consisting of occupied bonds (or sites) at random with a fixed probability (Stauffer, 1985).

The percolation approach has been applied in two different ways. In one of these, a portion of bonds in the given lattice is considered as pores and the occupied probability is related to the concept of porosity (Reyes, 1985). In the other, however, the overall lattice is occupied by pores (or pores/throats), and the intrusion and extrusion processes are envisioned as the formation of clusters for percolation theory (Lane et al., 1986). Our approach belongs to the former.

Although percolation theory is applied to an infinite lattice, in practice one should consider a lattice of finite size (Lopez et al., 1988). In this case the accessible probability is defined as the number fraction of the occupied bonds (or sites) connected to the external surface in the finite lattice (Conner and Lane, 1984; Lane et al., 1986).

Porous material could well be represented by a three-dimensional lattice such as simple cubic lattice. In this paper, however, a square lattice was used instead of a cubic one in view of the following arguments: The ratio of the number of exterior bonds to the total number of bonds is equal in both square and cubic lattices [if the number of sites in one direction is N, the

Correspondence concerning this paper should be addressed to Son-Ki Ihm.

ratio is $2/(N+1)$]. The necessary lattice should have a coordination number above 4 because the coordination number is about 4 in the random packing of glass spheres and the number will drop to a value about 3 for partially consolidated material (Mason, 1983). The coordination number in a square lattice is 6 for bond percolation, which covers the coordination number of 4.

The present work is aimed at analyzing hysteresis in mercury porosimetry using a finite square lattice for bond percolation. Hypotheses of no coalescence and no entrapment were introduced in mercury penetration, and their effects on hysteresis were investigated by taking the Rayleigh distribution function. In particular, the analysis focuses on predicting hysteresis with a little entrapment. The bimodal pore size distribution was analyzed by considering the extent of overlapping and the sequence of connection between the micropore and macropore size distributions. Also, the effect of entrapment on the hysteresis is taken into account by introducing as a parameter the pressure difference between the applied and assigned pressures as determined from the Washburn equation. The applicability of the proposed hypotheses is to be examined by correlating experimental data on the mercury penetration of α-alumina.

Hypotheses on Mercury Penetration

Two conditions for intrusion and extrusion processes must be satisfied:

1. A pore has interface(s) between gas and mercury
2. The pore radius is greater for intrusion, or smaller for extrusion, than that related through the Washburn equation to the applied pressure

In addition, for the extrusion process, a connected path of mercury must exist between the pore and the exterior surface (Reyes, 1985).

Consider a tentative pore structure as shown in Figure 1a. The sequence of relative size of pores is as follows: $r_1 < r_2 < r_3 < r_4 < r_5 < r_6$. In the intrusion step, the gas–mercury interface is located initially at the entrance of pore 4, which is the external pore of the cluster. Pore 4 is filled with mercury when the applied pressure is beyond its assigned pressure. The interface moves to the connection node of pores 1, 4, 5, and 6 and so pores 1, 5, and 6 become interfacial pores. Mercury will penetrate pores 5 and 6 first, which have larger radii than pore 4. The next intrusion will be the penetration into pore 3, and pore 2 will have two interfaces at both ends. After subsequent intrusion of mercury into pore 2, two interfaces still remain in the middle of pore 2; that is, both are not coalesced with each other. When the mercury intrudes into pore 1, which is the smallest and dead-end pore, a question arises if the two interfaces present in pore 2 coalesce and disappear. According to previous assumptions by others (Androutsopoulos and Mann, 1979; Reyes, 1985), interfaces remain at the pore intruded last in a cluster or at the dead-end pores. The pore intruded last has the uncoalesced interface at its central part, provided that it is not a dead-end pore. This could be called the hypothesis of coalescence. However we are proposing a hypothesis that a pore which joins a closed loop and is filled penultimately to a dead-end pore, can have an uncoalesced interface. An interface of course exists also at the dead-end pore. This will be called the hypothesis of no coalescence. As a result of this hypothesis, the number of the initial interfaces for extrusion increases. Thereby, pore 2 may have the interface because it is penetrated last in the closed loop consisting of pores 2, 3, 5, and 6.

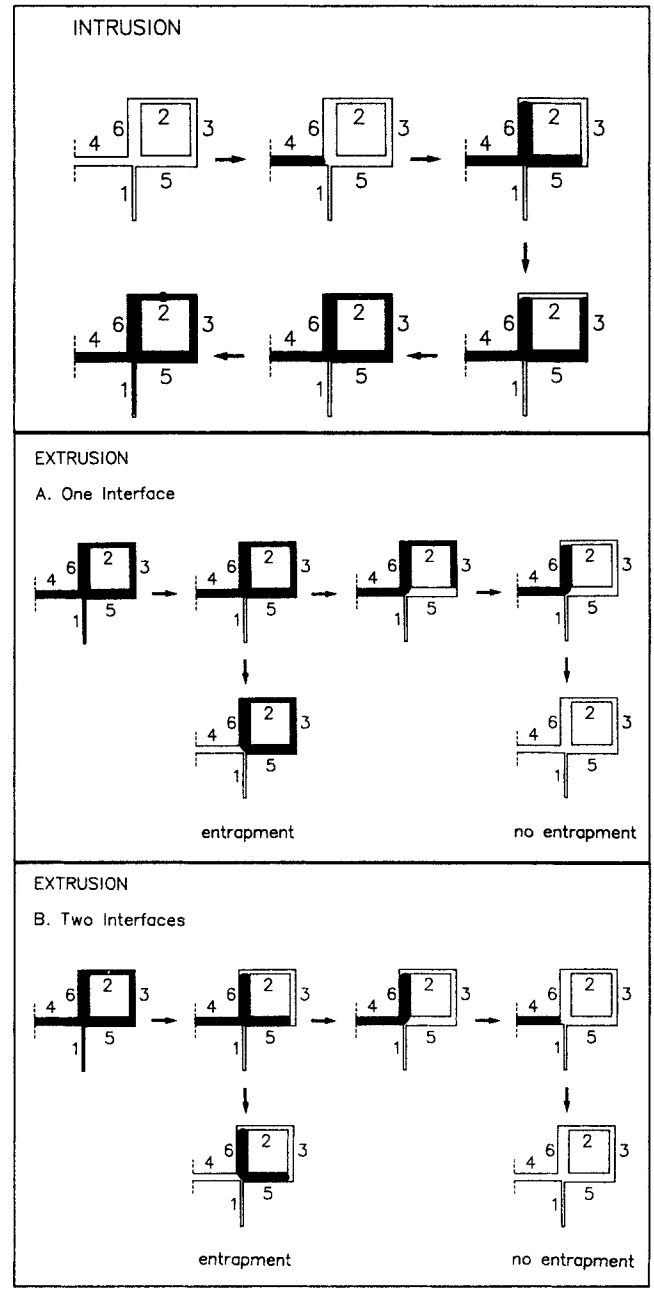

Figure 1. Intrusion and extrusion with the proposed hypotheses.

Several possibilities of no coalescence, though they are not envisioned clearly, can be recommended by the following arguments:

1. The residual amount of gas ultimately contained within the smallest pore in the closed loop will prevent coalescence from taking place (Androutsopoulos and Mann, 1979)
2. When the pressure is lowered, gas contained within the dead-end pores moves through the pore surface to the smallest pore in the closed loop
3. Micropores or crevices, which are not considered in the lattice, play the role of dead-end pores.

The second phenomenon is similar to snap-off at the inception of extrusion, which was investigated by Wardlaw and McKellar (1980). It is quite natural that this hypothesis will affect the interpretations of the hysteresis and entrapment in mercury porosimetry. Different types of hysteresis and entrapment can be predicted and it is hoped that more satisfactory explanations could be drawn from this hypothesis.

The hypothesis is more critical when the extrusion is considered. In the example of Figure 1b, the initial interface for extrusion is present only in pore 1 under the previous assumptions made by other investigators. After extrusion in pore 1, new interfaces are created in pores 4, 5, and 6. If the pressure decreases incrementally, pore 4 is easily drained and the other filled pores—2, 3, 5, and 6—are isolated (entrapment). On the other hand, using the hypothesis of no coalescence, an additional interface also exists in pore 2 as shown in Figure 1c and pores 2 and 3 are evacuated consecutively. Although mercury entrapment takes place in pores 5 and 6 by the drainage in pore 4, the extruded sequence and the amount of the entrapment are different from the above result based on the hypothesis of coalescence.

When pore sizes are distributed and pores are interconnected, some mercury penetration data show hysteresis without mercury entrapment. This is rather inexplicable with the previous assumption of coalescence. If the entrapment should disappear eventually—this will be called the hypothesis of no entrapment—extrusion results in different hysteresis, as shown in Figures 1b and 1c, even if the intrusion processes are the same. Under the hypothesis of coalescence and no entrapment, pores 5, 3, 2, 6, and 4 are drained sequentially after extrusion in pore 1, Figure 1b. Under the hypothesis of no coalescence and no entrapment, however, pores 3and 5 are extruded. Pore 4 will not be drained until the mercury is extruded from pore 6, which is the largest pore, Figure 1c. The correlation between entrapment and no entrapment may be needed to interpret the interrelation between hysteresis and entrapment. Therefore it is also proposed that the extent of entrapment is to be analyzed by a parameter, the pressure difference between the applied pressure and the pressure assigned (by the Washburn equation), which could be the measure of mercury breakage.

Modeling and Simulation Procedure

The pore structure of a porous material is envisioned as a square lattice composed of bonds occupied with a fixed probability (bond percolation). All occupied bonds are considered as pores of equal length. In this paper the probability, p, represents the accessible probability in the finite lattice (Lane et al., 1986; Lopez et al., 1988). The radius of each occupied bond is distributed according to the Rayleigh distribution function as follows:

$$f_R(r) = \frac{(r - r_m)}{(r_a - r_m)^2} \exp\left[-\frac{(r - r_m)^2}{2(r_a - r_m)^2}\right], \quad r > r_m$$

where r_a and r_m represent the average and the minimum radii, respectively. It should be stressed that any of other various distribution functions can be used for the pore size distribution. The decision can be made depending upon the apparent shape of penetration data. It is noted that Rayleigh distribution is a two-parameter function, slightly skewed toward small pore sizes and similar to the log normal distribution function, which is often a good estimation of pore size distribution in porous material.

The lattice size, probability, and other parameters related to pore size distribution are given initially. Accessible bonds are determined at random for the given probability. The probability assumed initially is chosen somewhat smaller than the given one in order to avoid overestimation. Using the classification routine of Stauffer (1985), the accessible bonds are sorted and the isolated bonds ignored. The above procedure is repeated until the exact number of accessible bonds is obtained. Each accessible bond is given its radius by the pore size distribution function. In the intrusion step, all bonds are initially checked to determine if they are present on the outer surface of the lattice, because the bonds on the outer surface of the lattice have the gas–mercury interfaces. The largest one of these interfacial bonds is selected. After the largest is invaded by bulk mercury, the neighboring bonds become interfacial ones. Searching for the largest interfacial bond is continued according to the aforementioned procedure. The subsequent pattern of mercury intrusion is determined by the applied pressure, pore radius, and the existence of interface. In the extrusion step, the bonds with initial interface designated by the hypothesis of no coalescence and the dead-end bonds are initially sorted out and the smallest pore could be evacuated. But if the bond makes the remaining bonds within the included cluster to become isolated, mercury within the bond cannot be drained due to the hypothesis of no entrapment. If a certain bond is drained, new interfaces are generated through the same procedure used in the intrusion step. The simulation procedure is discussed in more detail in the thesis by Park (1990).

The size of the square lattice was chosen as 10×10 sites and the total number of bonds in the lattice becomes 220 ($p = 1.0$). In each calculation the number of repetitions was determined such that the product of the number of occupied bonds and the repetitions is in the range of 8,500 to 10,000. This was necessary to give similar error bounds to a given distribution function for different values of accessible probability. For example, 400 repetitions were needed for $N = 10$ and $p = 0.1$.

Results and Discussion

Variation with hypotheses for Rayleigh distribution

Figure 2 shows the result on Rayleigh pore size distribution with $r_m = 20$ nm and $r_a = 40$ nm, where the central solid line represents the true size distribution based on the capillary tube model (no hysteresis). At a probability of 0.4, the hysteresis and entrapment varied depending upon the assumptions used, as shown in Figure 2. Under the hypothesis of coalescence and entrapment (dashed line), the width of the hysteresis loop is the largest. In contrast, hysteresis loop width is smallest under the hypothesis of no coalescence and no entrapment (solid line). With the coalescence of interfaces, the extrusion steps are more delayed at the inception, but the extent of entrapment is diminished.

The hysteresis loop would become more wider and extrusion curves would be more delayed if the hysteresis of contact angle were considered in addition to the interconnection of pores (Larson et al., 1981; Lowell and Shields, 1982; Kloubek, 1983; Conner et al., 1984). However, the hysteresis of contact angle is not related to pore interconnection and should be treated independently (Reyes, 1985).

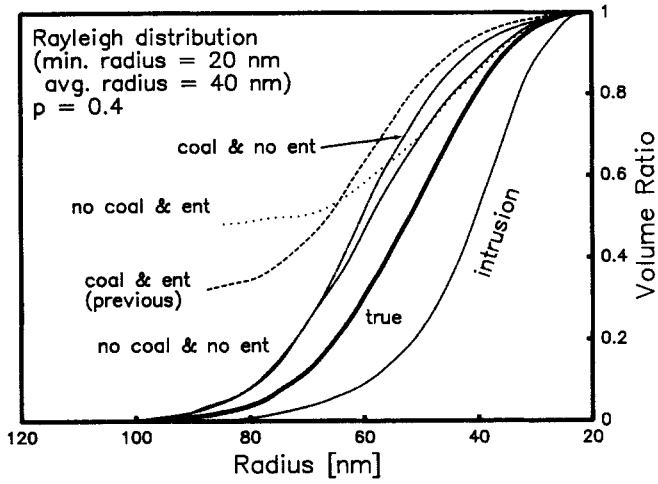

Figure 2. Prediction of hysteresis and entrapment with the proposed hypotheses.

Hysteresis phenomenon

As shown in Figure 3, hysteresis varied with probability on Rayleigh distribution with $r_m = 20$ nm and $r_a = 40$ nm. Initially, mercury intrusion takes place in the lattice boundary. The mercury intrusion is delayed because only a portion of large pores exists on the boundary and so most of the large bonds are not intruded by mercury at these assigned pressures. The obtained pore size distribution based on the intrusion process then shifts toward the smaller radius, away from the true one.

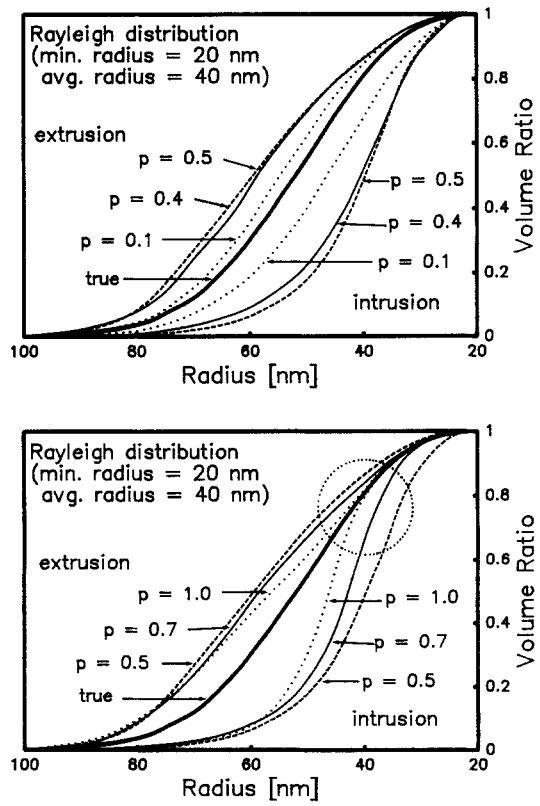

Figure 3. Prediction of intrusion and extrusion with accessible probability p.

In the extrusion step, the initial interfaces exist within bonds that are dead-end bonds and the bonds intruded last in the closed loop according to the hypothesis of no coalescence. But the extrusion process is also delayed because many small bonds do not have interfaces at these assigned pressures.

Effects of probability

The porosimetry process may be divided into two groups of probability. The first group is the lower probability region between 0.0 and 0.5; the second is the larger probability region between 0.5 and 1.0. The deviation from the capillary tube model increases with increasing p in the first group as shown in Figure 3a, and the intrusion and extrusion curves are quite close over the range of small pores in the second group, as indicated by a dotted circle in Figure 3b.

In order to show the effect of probability on hysteresis more explictly, in Figure 4 dimensionless extruded volume has been plotted vs. dimensionless intruded volume based on the total intruded volume. The dashed diagonal line represents the case without hysteresis. The deviation between each curve and this line corresponds to the width of each hysteresis loop. The deviation at $p = 0.4$ is wider than that at $p = 0.1$. At $p = 0.7$ and $p = 1.0$, the curves are inflected and then bent to the diagonal.

Variation with pore size distribution

Five different Rayleigh distributions are considered and the values of $r_m = 20$ nm and $r_a = 40$ nm are taken as the basis. Skewness is considered by varying the value of r_m, for example, to 5 nm or 35 nm. Also, the distributed ranges of pore size are moved toward smaller or larger size, such as $r_m = 0$ nm and $r_a = 20$ nm, or $r_m = 40$ nm and $r_a = 60$ nm.

Figure 5 shows the effects of skewness and average radius at $p = 0.4$ where the width of the hysteresis loop is wide enough to consider the above effect. In Figure 5a, the width of the hysteresis loop becomes wider with increasing skewness but seems to be independent of the probability. Under the condition of the same skewness, the width is insensitive to the variation of average radius, as shown in Figure 5b. But if the probability of porous material is not known, the probability cannot be obtained from a figure such as Figure 5.

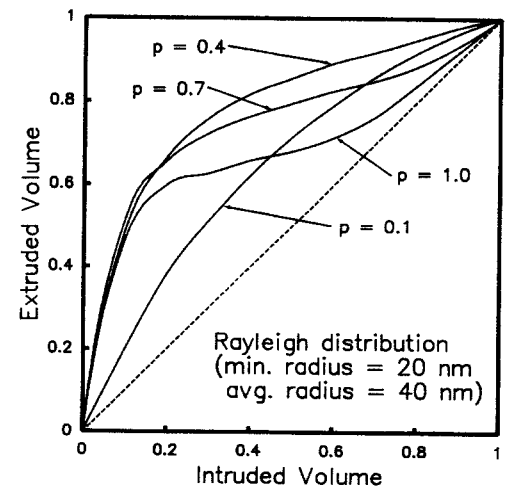

Figure 4. Plot of dimensionless volume.

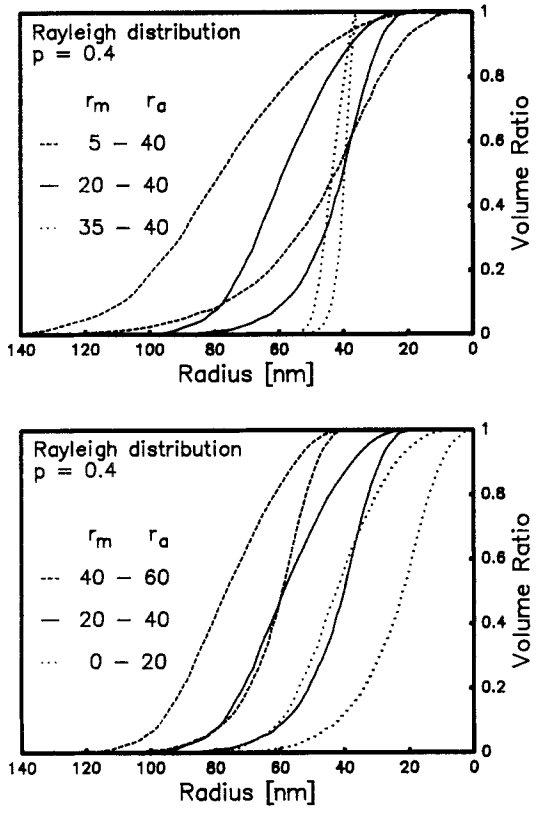

Figure 5. Prediction of intrusion and extrusion.

In Figure 6 the relative distances between curves at $p = 0.7$ are wider than those at $p = 0.4$ but the relative sequences are the same at both probabilities. All curves at $p = 0.7$ are inflected. Also, the deviation of each curve from a diagonal line becomes larger with increasing skewness or with shifting the distribution toward the range of small size.

Because the types of curves vary seriously with p as described in Figures 4 and 6, the probability can be obtained tentatively from the plot of dimensionless volume. It has been confirmed by the authors that the effects of accessible probability are predominant also for other distribution functions such as log normal, normal, and square distributions (Park, 1990).

Bimodal pore size distribution

Porous material such as pelletized catalyst shows a bimodal pore size distribution consisting of micropores and macropores. The relative ranges and the sequence of connection between both distributions are believed to affect the hysteresis and entrapment.

The size distributions of micropores and macropores were again assumed to Rayleigh distribution functions. The accessible probability was selected to be 0.4 where the hysteresis loop was wide enough. The Rayleigh distribution for the micropores was assumed to have $r_m = 10$ nm and $r_a = 20$ nm. The number ratio of micropores to macropores was taken as 4 in order to balance the contribution of the micropores to porosity.

In considering the extent of overlapping, the micropore size distribution was fixed and the Rayleigh distributions for the macropore distributions were chosen as follows:

$r_m = 20$ nm, $r_a = 30$ nm—complete overlapping
$r_m = 40$ nm, $r_a = 50$ nm—partial overlapping
$r_m = 60$ nm, $r_a = 70$ nm—completely separated

Two types of connection sequence, independent and random, were considered between both distributions. Independent connection, which was described as a type of nonrandom heterogeneity (Wardlaw and McKellar, 1980) or of nonrandomness (Lane et al., 1986), is composed of trunklike macropores and branchlike micropores. After macropores are distributed accessibly, micropores can be connected to macropores and/or other micropores. When the porous material is made of microporous powder through pelletizing or a packing process, independent connection is expected. In random connection, all pores are distributed randomly.

Figure 7a shows the effects of the extent of overlapping on hysteresis for independent connection. When the distributions of macropore and micropore sizes are separated (solid curve), the process has two independent hysteresis curves. One is ranged in

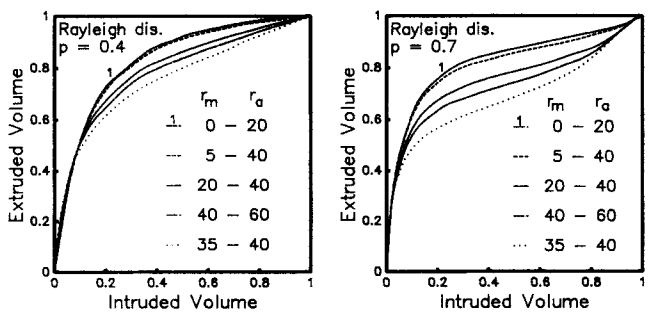

Figure 6. Plots of dimensionless volume.

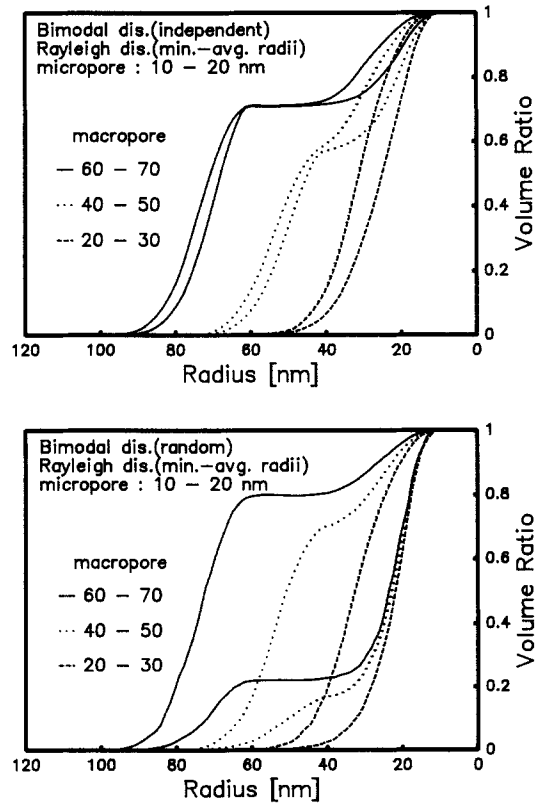

Figure 7. Effects of extent of overlapping on hysteresis.

the micropore region and the other in the macropore region. It is presumed that this result corresponds to the case of physical mixture of microporous medium and macroporous medium. It seems that good correlation could be obtained for the "separated and independent" experimental data. As the extent of overlapping increases, both hysteresis curves are also overlapped. In random connection, the hysteresis loop is much wider than that in independent connection, as shown in Figure 7b. It can be shown that random connection has less intrusion for macropores and also a smaller extrusion for micropores than does independent connection.

Entrapment

If the bulk mercury and an interfacial large pore are connected to each other by an interfacial small pore, it is believed that energy is needed for mercury breakage (or snap-off) within the small pore beyond the cohesive force (Lowell, 1980). Whether mercury breakage takes place or not can be established by comparing the energy required to break the mercury column with the pore potential at the present applied pressure. Pore potential at the applied pressure can be considered as the pressure difference between the assigned and the applied pressures. If the pressure difference is beyond the critical value of a requisite energy for breakage, the mercury within the small pore can be withdrawn and the large pore is disconnected and isolated from the bulk mercury. Accordingly, the extent of entrapment could be simulated by taking the critical pressure difference (CPD) as a parameter.

The CPD is initially imposed on simulation, and whether the mercury within a bond is drained or not is determined by comparing the difference between applied and assigned pressures with the given CPD. When the bonds are isolated, the mercury within these bonds is considered to be entrapped.

Entrapment, which has been investigated by others (Androutsopoulos and Mann, 1979; Reyes, 1985), corresponds only to the case of CPD = 0 with coalescence. If the value of CPD is infinite, mercury entrapment will not be expected, irrespective of coalescence. Figure 8a shows the result of CPD = 0, 4,000, 8,000 kPa and infinite value (no entrapment) at $p = 0.4$. The extent of entrapment is reduced with increasing critical pressure difference. Also, as the probability increases up to 0.6, the amount of entrapment increases for CPD = 0 kPa. Above a probability of 0.7, entrapment decreases a little, as shown in Figure 8b.

Experimental correlation

By considering the analysis of bimodal distribution, it is believed that the applicability of the proposed hypotheses may be better demonstrated when micro- and macropores are completely separated and the connection is independent.

In independent connection, the powders of α-alumina were molded into pellets, which are expected to have a bimodal pore size distribution. The α-alumina powders (450–670 nm in size) were made into a paste with water. The paste was pelletized and the pellets were calcined in air at 1,400°C. Sample particles of 3 mm size were prepared by crushing the pellets. Mercury penetration was measured by using Auto-pore 9200 (Micromeritics Instrument Corp.) where maximum applied pressure was 42,000 kPa. The values of surface tension, δ, and contact angle, θ, were taken as 4.85 N/m and 140°, respectively.

Figure 9 shows the volume ratio of porosimetry of α-alumina

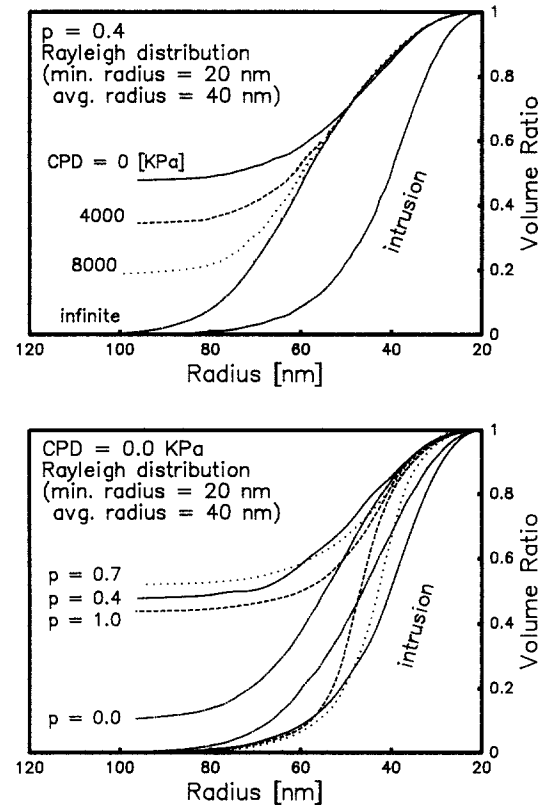

Figure 8. Effects of critical pressure difference and probability on entrapment.

particles. Although the extent of entrapment is about 75%, it is clearly seen that the pore size distribution is bimodal. Moreover, the micropores are separated and the hysteresis loop for micropores is independent. The micropores may be analyzed by using the proposed hypotheses of no coalescence and no entrapment.

Intrusion and extrusion data can be correlated by log normal distribution functions. The log normal distribution function, which can be skewed significantly toward small sizes, is given as

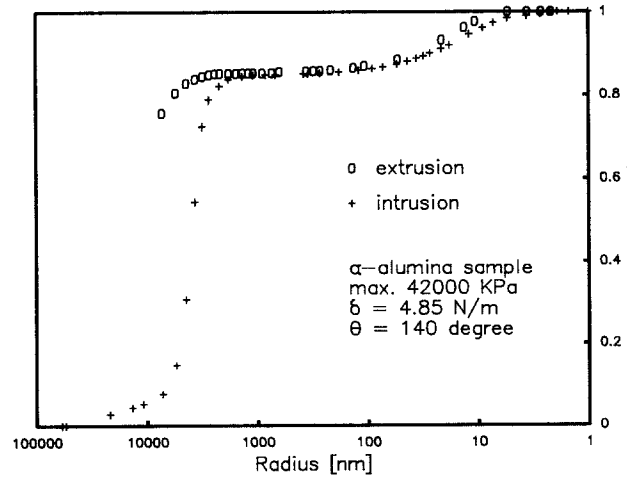

Figure 9. Experimental data of mercury intrusion and extrusion for α-alumina.

follows:

$$f_L(r) = \frac{1}{r\sigma(2\pi)^{1/2}} \exp\left[-\frac{[\ln (r/r_a)]^2}{2\sigma^2} \right], \quad 0 < r < \infty$$

Intrusion data are well correlated with $r_a = 5$ nm and $\sigma = 0.7$, and extrusion data with $r_a = 15$ nm and $\sigma = 0.5$. These two distributions make the upper and lower bounds for the true distribution. It has been suggested that the true pore size distribution, being always between the two distributions, covers the range of small pore sizes for intrusion process and the range of large pore sizes for extrusion process. With this in mind, the following three log normal distribution functions were tested for the true micropore size distribution:

$r_a = 7$ nm, standard deviation $\sigma = 0.8$
$r_a = 8$ nm, $\sigma = 0.7$
$r_a = 9$ nm, $\sigma = 0.6$

The accessible probabilities must be determined for each of the selected distributions. This can be done through the dimensionless plot for intruded and extruded volume, shown in Figure 10. As discussed previously, the curves in this dimensionless plot are affected mainly by the accessible probability. The accessible probability can be taken as 0.05 in this particular case, and this seems reasonable since the porosity of α-alumina is known to be very small. Once the accessible probability is given, the parameter estimation for the log normal distribution function can be made through a nonlinear regression under the criterion of minimizing the sum of squares. The case of log normal distribution with $r_a = 8$ nm, $\sigma = 0.7$ was chosen a priori to meet the criterion. It can be seen in Figure 11 that this case best fits the data.

Conclusions

Mercury porosimetry was analyzed by percolation theory, for which new hypotheses of no coalescence and no entrapment were proposed. It was demonstrated how the new hypotheses affect the hysteresis loop of intrusion and extrusion. With increasing accessible probability, the hysteresis loop becomes wider for a lower probability region, between 0 and 0.5, and narrower for a higher probability region, between 0.5 and 1.0. Especially in the range of $p > 0.5$, the extrusion curves were closer to the intrusion curves for smaller pores. It is noted that hysteresis without entrapment, which has not been simulated by previous works when the pore sizes are distributed and pores are interconnected, can be predicted through the new hypotheses. For a bimodal pore size distribution consisting of micro- and macropores, the effects of both extent of overlapping and sequence of connection on hysteresis were analyzed. It was also shown that mercury entrapment can be predicted by considering the pressure difference between the applied and assigned pressures as a parameter for mercury breakage. Finally, it was demonstrated that the micropore size distribution of α-alumina can be correlated by using the present model with the new hypotheses. In summary, this paper shows that a complex lattice model is not necessary to demonstrate hysteresis and mercury entrapment in porosimetry. Even a modest two-dimensional model can demonstrate these phenomena. In particular, hysteresis is a consequence of sequential intrusion and extrusion, and entrapment may be explained by mercury breakage during the extrusion process for this model.

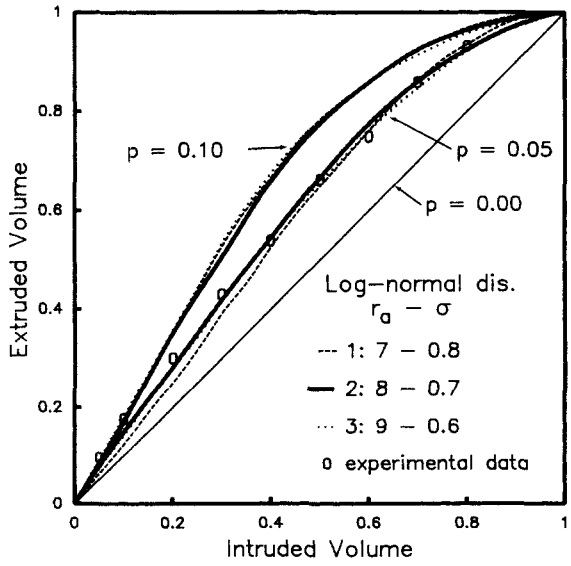

Figure 10. Plot of dimensionless volumes for log normal pore size distributions.

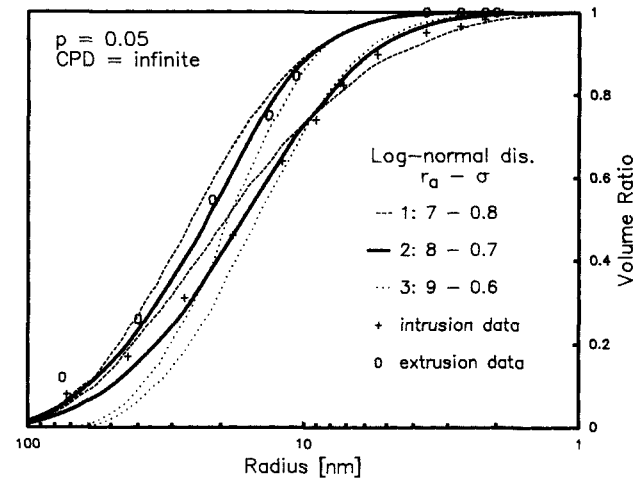

Figure 11. Comparison between experimental data and result of simulation for micropore size distribution.

Notation

CPD = critical difference between applied and assigned pressures, kPa
CTM = capillary tube model
f_R = Rayleigh distribution function
f_L = log normal distribution function
N = lattice size
P = applied pressure, kPa
p = accessible probability
r = pore radius, nm
r_a = average radius, nm
r_m = minimum radius, nm

Greek letters

δ = surface tension, N/m
θ = contact angle, degree
σ = standard deviation

Literature Cited

Androutsopoulos, G. P., and R. Mann, "Evaluation of Mercury Porosimeter Experiments Using a Network Pore Structure Model," *Chem. Eng. Sci.*, **34,** 1203 (1979).

Broadbent, S. R., and J. M. Hammersley, "Percolation Processes. I: Crystals and Mazes," *Proc. Camb. Phil. Soc.*, **53,** 629 (1957).

Conner, W. C., and A. M. Lane, "Measurement of the Morphology of High Surface Area Solids: Effect of Network Structure on the Simulation of Porosimetry," *J. Catal.*, **89,** 217 (1984).

Conner, W. C., A. M. Lane, and A. J. Hoffman, "Measurement of the Morphology of High Surface Area Solids: Hysteresis in Mercury Porosimetry," *J. Colloid Interf. Sci.*, **100,** 185 (1984).

Dullien, F. A. L., *Porous Media: Fluid Transport and Pore Structure,* Academic Press, New York (1979).

Essam, J. W., "Percolation Theory," *Rep. Prog. Phys.*, **43,** 833 (1980).

Kloubek, J., "Volume and Contact Angle Hystereses in Mercury Porosimetry of ASC-Whetlerite," *J. Colloid Interf. Sci.*, **95,** 135 (1983).

Lane, A., N. Shah, and W. C. Conner, "Measurement of the Morphology of High Surface Area Solids: Porosimetry as a Percolation Process," *J. Colloid Interf. Sci.*, **109,** 235 (1986).

Larson, R. G., L. E. Scriven, and H. T. Davis, "Percolation Theory of Two-Phase Flow in Porous Media," *Chem. Eng. Sci.*, **36,** 57 (1981).

Lopez, I., J. C. de la Cal, M. Montes, and J. M. Asua, "A Percolation Model of Impregnation of Porous Supports under Diffusional Control," *Proc. 9th Int. Cong. Catal.*, 1920 (1988).

Lowell, S., "Continuous-Scan Mercury Porosimetry and the Pore Potential as a Factor in Porosimetry Hysteresis," *Powder Technol.*, **25,** 37 (1980).

Lowell, S., and J. E. Shields, "Influence of Pore Potential on Hysteresis and Entrapment in Mercury Porosimetry," *J. Colloid Interf. Sci.*, **90,** 203 (1982).

Mason, G., "The Effect of Pore Space Connectivity on the Hysteresis of Capillary Condensation in Adsorption–Desorption Isotherms," *J. Colloid Interf. Sci.*, **88,** 36 (1982).

———, "The Effect of Pore Lattice Structure on the Pore Size Distributions Calculated from Sorption Isotherms Using Percolation Theory," *J. Colloid Interf. Sci.*, **95,** 277 (1983).

Mishra, B. K., and M. M. Sharma, "Measurement of Pore Size Distributions from Capillary Pressure Curves," *AIChE J.*, **34,** 684 (1988).

Park, C. Y., "Analyses on the Pore Size Distribution and the Free Radical Polymerization through Percolation Theory," Ph.D. Diss., Korea Advanced Inst. Sci. Technol. (1990).

Rafi, F., and M. Tirrell, "Percolation in Catalytic Porous Media with Application to Polymerization," *AIChE J.*, **34,** 698 (1988).

Reyes, S. C., "Applications of Percolation Theory to Modeling of Noncatalytic Gas–Solid Reactions," Ph.D. Diss., Univ. Minnesota (1985).

Shante, V. K. S., and S. Kirkpatrick, "An Introduction to Percolation Theory," *Adv. Phys.*, **20,** 325 (1971).

Stauffer, D., *Introduction to Percolation Theory,* Taylor and Francis, London (1985).

Wall, G. C., and R. J. C. Brown, "The Determination of Pore Size Distributions from Sorption Isotherms and Mercury Penetration in Interconnected Pores: The Application of Percolation Theory," *J. Colloid Interf. Sci.*, **82,** 141 (1981).

Wardlaw, N. C., and M. McKellar, "Mercury Porosimetry and the Interpretation of Pore Geometry in Sedimentary Rocks and Artificial Models," *Powder Technol.*, **29,** 127 (1981).

Yanuka, M., F. A. L. Dullien, and D. E. Elrick, "Percolation Processes and Porous Media. I: Geometrical and Topological Model of Porous Media Using a Three-Dimensional Joint Pore Size Distribution." *J. Colloid Interf. Sci.*, **112,** 24 (1986).

Zhdanov, V. P., V. B. Fenelonov, and D. K. Efremov, "Determination of Pore Size Distribution from Sorption Isotherms: Application of Percolation Theory," *J. Colloid Interf. Sci.*, **120,** 218 (1987).

Manuscript received Apr. 20, 1990, and revision received Aug. 20, 1990.